Ordered Mesoporous SiOC and SiCN Ceramics from Atmosphere-Assisted in Situ Transformation

Yifeng Shi, Ying Wan, Yunpu Zhai, Ruili Liu, Yan Meng, Bo Tu, and Dongyuan Zhao*

Department of Chemistry, Shanghai Key Laboratory of Molecular Catalysis and Innovative Materials, Key Laboratory of Molecular Engineering of Polymers, Advanced Materials Laboratory, Fudan University, Shanghai 200433, People's Republic of China

Received January 30, 2007

An atmosphere-assisted heating process was utilized to transform mesostructured SiC−C nanocomposites in situ into ordered mesoporous SiOC and SiCN ceramics with relatively small structural shrinkage. The mesostructured SiC−C nanocomposites were fabricated using commercially available polycarbosilane (PCS) as a ceramic precursor and mesoporous carbon CMK-3 as a hard template that itself was prepared by a nanocasting procedure from mesoporous silica SBA-15. Reactive gases including air and ammonia were employed to simultaneously incorporate O or N into SiC ceramics and oxidize or reduce the carbon template and excess carbon deposits. The procedure was carried out at 500 °C for 10 h and at 1000 °C for 10 h for air- and ammonia-assisted in situ transformations, respectively. SAXS, XRD, N_2 sorption, and TEM analyses revealed that the mesoporous SiOC and SiCN ceramics exhibit open, continuous frameworks similar to that of the primary template ordered mesoporous SBA-15. The ordered mesoporous SiOC and SiCN ceramics have high surface areas (200−400 $m^2\ g^{-1}$), large pore volumes (0.4−0.8 $cm^3\ g^{-1}$), and narrow pore size distributions (4.9−10.3 nm). The structural shrinkage from mesostructured SiC−C composites to mesoporous SiC-based ceramics decreased with increasing initial pyrolysis temperature for SiC−C nanocomposites owing to the improvement of structural rigidity. This shrinkage was found to be as low as 2.6% from mesostructured SiC−C pyrolysis at 1400 °C to mesoporous SiCN-1400 via ammonia-assisted in situ transformation.

1. Introduction

Advances in materials fabrication, including those enabled by nanotechnology, have required the integration of components and features with pore structures. Silicon carbides exhibit unique chemical, thermal, and mechanical properties and are widely used as abradants, heater blocks, reinforced materials, optical materials, and semiconductor materials.[1,2] Introducing a third component, such as oxygen, nitrogen, boron, titanium, aluminum, or zirconium, into the SiC network can yield various SiC-based materials and efficiently improve their properties.[3−7] For example, the oxidation resistance is enhanced in silicon oxycarbide (SiOC) and carbonitride (SiCN) ceramics owing to the complex-covalent chemical bonds formed. Nanoporous SiC-based ceramics with high surface areas and large pore volumes have physical properties far different from those of the solid bulk materials. These materials have exhibited current and potential applications in electric devices,[8] blue-emitting diodes,[9] UV photodetectors,[10] catalysis,[11] biomaterials,[12] and separations.[13] The enhancement of these properties has been attributed to the confined-space effect in nanospace. Therefore, mesoporous SiC-based ceramics (e.g., SiOC and SiCN) with ordered mesostructures and tunable compositions have attracted increasing interest in recent research.

With these demands, many approaches and combinations of approaches have been developed in both design and fabrication processes. Nanoporous SiC-based materials are difficult to obtain because of their high formation temperatures. Disordered nanoporous silicon carbide ceramics can be fabricated by a solid−gas reaction of ordered mesoporous carbon replica with silicon vapor[14] and a chemical vapor infiltration of dimethyldichlorosilane inside mesoporous silica followed by the removal of silica.[15] Recently, highly ordered

* To whom correspondence should be addressed. Tel.: 86-21-6564-2036. Fax: 86-21-6564-1740. E-mail: dyzhao@fudan.edu.cn.

(1) Powell, A. R.; Rowland, L. B. *Proc. IEEE* **2002**, *90*, 942.
(2) Pensl, G.; Choyke, W. J. *Physica B* **1993**, *185*, 264.
(3) Matsuura, H.; Aso, K.; Kagamihara, S.; Iwata, H.; Ishida, T.; Nishikawa, K. *Appl. Phys. Lett.* **2003**, *83*, 4981.
(4) Samanta, A. K.; Dhargupta, K. K.; Ghatak, S. *J. Eur. Ceram. Soc.* **2000**, *20*, 1883.
(5) Weinmann, M.; Schuhmacher, J.; Kummer, H.; Prinz, S.; Peng, J. Q.; Seifert, H. J.; Christ, M.; Muller, K.; Bill, J.; Aldinger, F. *Chem. Mater.* **2000**, *12*, 623.
(6) Soraru, G. D.; Suttor, D. *J. Sol-Gel Sci. Technol.* **1999**, *14*, 69.
(7) Karmann, S.; Suttrop, W.; Schoner, A.; Schadt, M.; Haberstroh, C.; Engelbrecht, F.; Helbig, R.; Pensl, G.; Stein, R. A.; Leibenzeder, S. *J. Appl. Phys.* **1992**, *72*, 5437.
(8) Connolly, E. J.; O'Halloran, G. M.; Pham, H. T. M.; Sarro, P. M.; French, P. J. *Sens. Actuator A: Phys.* **2002**, *99*, 25.
(9) Liao, L. S.; Bao, X. M.; Yang, Z. F.; Min, N. B. *Appl. Phys. Lett.* **1995**, *66*, 2382.
(10) Afanas'ev, A. V.; Il'in, V. A.; Korovkina, N. M.; Savenko, A. Y. *Tech. Phys. Lett.* **2005**, *31*, 629.
(11) Keller, N.; Pham-Huu, C.; Crouzet, C.; Ledoux, M. J.; Savin-Poncet, S.; Nougayrede, J. B.; Bousquet, J. *Catal. Today* **1999**, *53*, 535.
(12) Rosenbloom, A. J.; Sipe, D. M.; Shishkin, Y.; Ke, Y.; Devaty, R. P.; Choyke, W. J. *Biomed. Microdevices* **2004**, *6*, 261.
(13) Kim, Y.; Kim, S. R.; Cho, K. H.; Bae, S. Y.; Kwon, W. T. In *Eco-Materials Processing & Design VII*; Kim, H. S., Li, Y. B., Lee, S. W., Eds.; Trans Tech Publications Ltd.: Zurich, Switzerland, 2006; Vols. 510−511, p 926.
(14) Liu, Z. C.; Shen, W. H.; Bu, W. B.; Chen, H. R.; Hua, Z. L.; Zhang, L. X.; Li, L.; Shi, J. L.; Tan, S. H. *Microporous Mesoporous Mater.* **2005**, *82*, 137.

10.1021/cm070283v CCC: $37.00
Published on Web 03/08/2007

mesoporous SiC materials with uniform pore sizes and ultralarge surface areas were synthesized by fully impregnating polycarbosilane (PCS) inside the channels of mesoporous silicates, annealing the samples, and then removing the hard templates of silicates.[16−18] This nanocasting strategy has proved to provide a general approach to the fabrication of mesoporous materials with diverse components. However, the reactivity of the silica matrix at high temperatures brings impurities into the final products. For example, silica can react with excess carbon to form SiO gas, and it can further react with carbon or nitrogen to form isolated SiC or Si_3N_4 beyond the mesostructure. Second, a high temperature is desired to improve the crystallinity of ceramics, but the flexibility and crystallization behavior of the silica matrix itself can decrease the structural regularity and increase the structural shrinkage. Moreover, this kind of replica material is constructed by nanowire arrays and connected by nanorods, which typically face the problems of mechanical instability because of the irregular and weak connection between the nanowires.

To obtain an open and integrated mesoporous SiC framework, a sol−gel process from tetraethyl orthosilicate (TEOS) and phenolic resin in the absence of surfactants has been attempted.[19] However, the resulting products were disordered, and the pore size distributions were broad. The surfactant-templating approach is normally used to synthesize highly ordered mesoporous oxides on the basis of the interactions between surfactants and precursors and between themselves. This, therefore, limits the synthesis to components with controllable sol−gel processes. To date, only a few examples have been given for SiC-based materials from the surfactant-templating approach. Co-assembly of a laboratory-made block copolymer and Ceraset led to mesoporous SiCN materials, which apparently had ultrahigh thermal stability (1500 °C).[20] However, the surface areas of the products were as low as about 51 $m^2\ g^{-1}$. Mesoporous SiOC materials have been prepared by directly treating mesostructured surfactant/organosilica/silica composites[21] and periodic mesoporous organosilicas (PMOs)[22] in inert atmosphere. Less than 2.3 wt % carbon was incorporated into the silica networks as estimated from their ^{29}Si nuclear magnetic resonance (NMR) spectra. A casting-by-casting method also provides an approach to give mesoporous ceramics with open frameworks. Ordered mesoporous carbon replicas casted from mesoporous silicates are used as the hard templates. The final goal materials replicate the pore topologies of these carbons and have almost the same frameworks as the original mesoporous silica scaffolds. This concept avoids the interactions between precursors and surfactants. Therefore, it can widen the viable mesoporous components,[23−31] especially for those that cannot be synthesized or are difficult to synthesize by the surfactant-templating approach. Miele and co-workers employed this casting-by-casting method to synthesize mesoporous BN materials using tri(methylamino)borazine as a precursor. The high-temperature ammonia treatment was first adopted to remove the mesoporous carbon template, which offered a new route in the removal of carbon template for the oxygen-sensitive materials.[24] It was also noticed that, when mesoporous silica and PMOs were treated by ammonia at high temperature, mesoporous silicon oxynitride and periodic mesoporous aminosilicas (PMAs) were obtained with the incorporation of nitrogen atoms in the framework.[32,33] This atmosphere-assisted in situ transformation strategy extends the composition of mesoporous family members.

In this article, we describe the fabrication of ordered mesoporous silicon oxycarbide and carbonitride ceramics with high surface areas through a combination of the casting-by-casting method with atmosphere-assisted in situ transformation. Ordered mesoporous carbon replicas casted from mesoporous silicates were chosen here as the hard templates, to produce SiC-based materials with open, continuous frameworks. Compared to mesoporous silica hard templates, carbon has the advantages of chemical inertness to SiC and stability even up to 1400 °C without marked structural shrinkage or crystallization behavior. Commercially available PCS, which has been reported to be quite suitable for the preparation of highly ordered mesoporous silicon carbides,[16−18] was used as the ceramic precursor. The similar surface C−H groups of PCS and mesoporous carbon might promote the interactions and facilitate the filling of guest molecules into the mesoporous space. After being annealed under nitrogen atmosphere at 900−1500 °C, mesostructured SiC−C nanocomposites were first prepared from PCS−C nanocomposites via solid-state thermolysis. The heating temperature and time for the subsequent atmosphere-assisted in situ transformation were found to be crucial for the formation of ordered mesoporous SiOC and SiCN ceramics. Air and ammonia atmosphere-assisted in situ transformations from mesostructured SiC−C composites to highly ordered mesoporous ceramics were carried out at 500 °C for 10 h and at 1000 °C for 10 h, respectively. This process involves the reaction between SiC frameworks and oxygen or ammonia and the

(15) Krawiec, P.; Weidenthaler, C.; Kaskel, S. *Chem. Mater.* **2004**, *16*, 2869.
(16) Shi, Y. F.; Meng, Y.; Chen, D. H.; Cheng, S. J.; Chen, P.; Yang, T. F.; Wan, Y.; Zhao, D. Y. *Adv. Funct. Mater.* **2006**, *16*, 561.
(17) Yant, J.; Wang, A. J.; Kim, D. P. *J. Phys. Chem. B* **2006**, *110*, 5429.
(18) Krawiec, P.; Geiger, D.; Kaskel, S. *Chem. Commun.* **2006**, 2469.
(19) Jin, G. Q.; Guo, X. Y. *Microporous Mesoporous Mater.* **2003**, *60*, 207.
(20) Kamperman, M.; Garcia, C. B. W.; Du, P.; Ow, H. S.; Wiesner, U. *J. Am. Chem. Soc.* **2004**, *126*, 14708.
(21) Nghiem, Q. D.; Cho, S. J.; Kim, D. P. *J. Mater. Chem.* **2006**, *16*, 558.
(22) Toury, B.; Blum, R.; Goletto, V.; Babonneau, F. *J. Sol-Gel Sci. Technol.* **2005**, *33*, 99.
(23) Roggenbuck, J.; Tiemann, M. *J. Am. Chem. Soc.* **2005**, *127*, 1096.
(24) Dibandjo, P.; Bois, L.; Chassagneux, F.; Cornu, D.; Letoffe, J. M.; Toury, B.; Babonneau, F.; Miele, P. *Adv. Mater.* **2005**, *17*, 571.
(25) Liu, Q.; Wang, A. Q.; Wang, X. D.; Zhang, T. *Chem. Mater.* **2006**, *18*, 5153.
(26) Lu, A. H.; Schmidt, W.; Taguchi, A.; Spliethoff, B.; Tesche, B.; Schuth, F. *Angew. Chem., Int. Ed.* **2002**, *41*, 3489.
(27) Kang, M.; Yi, S. H.; Lee, H. I.; Yie, J. E.; Kim, J. M. *Chem. Commun.* **2002**, 1944.
(28) Kim, J. Y.; Yoon, S. B.; Yu, J. S. *Chem. Mater.* **2003**, *15*, 1932.
(29) Lu, A. H.; Schmidt, W.; Spliethoff, B.; Schuth, F. *Chem.-Eur. J.* **2004**, *10*, 6085.
(30) Sakthivel, A.; Huang, S. J.; Chen, W. H.; Lan, Z. H.; Chen, K. H.; Kim, T. W.; Ryoo, R.; Chiang, A. S. T.; Liu, S. B. *Chem. Mater.* **2004**, *16*, 3168.
(31) Fang, Y. M.; Hu, H. Q. *J. Am. Chem. Soc.* **2006**, *128*, 10636.
(32) Xia, Y. D.; Mokaya, R., *Angew. Chem., Int. Ed.* **2003**, *42*, 2639.
(33) Asefa, T.; Kruk, M.; Coombs, N.; Grondey, H.; MacLachlan, M. J.; Jaroniec, M.; Ozin, G. A. *J. Am. Chem. Soc.* **2003**, *125*, 11662.

simultaneous removal of the carbon. A small structural shrinkage can result when the mesostructured SiC−C has a rigid framework. The ordered mesoporous SiOC and SiCN products obtained are thermally stable and have high surface areas (200−400 $m^2\ g^{-1}$), large pore volumes (0.4−0.8 $cm^3\ g^{-1}$), and narrow pore size distributions (4.9−10.3 nm).

2. Experimental Section

2.1. Chemicals. Triblock poly(ethylene oxide)-*b*-poly(propylene oxide)-*b*-poly(ethylene oxide) copolymer Pluronic P123 (M_w = 5800, $EO_{20}PO_{70}EO_{20}$) was purchased from Aldrich Chemical Inc. Polycarbosilane (PCS, M_n = 1500, yield point = 218−247 °C) was obtained from Key Lab of Ceramic Fiber and Composites, National University of Defense Technology (Changsha, People's Republic of China). Other chemicals were purchased from Shanghai Chemical Company. All chemicals were used as received without any further purification. Millipore water was used in all experiments.

2.2. Synthesis of Hard Templates. Mesoporous silica SBA-15 hard template was prepared by a hydrothermal synthesis method with the hydrothermal treatment at 100 °C for 24 h according to established procedures.[34] Mesoporous carbon CMK-3 was synthesized by the nanocasting process using sucrose as a precursor and mesoporous silica SBA-15 as a hard template according to the literature.[35] First, 22.5 g of sucrose was added to a mixture of 108 g of H_2O and 2.52 g of H_2SO_4 (98 wt %) with stirring. After the sucrose had dissolved completely, 18.0 g of SBA-15 was added. The mixture was stirred until the water had nearly evaporated and was subsequently heated in an oven at 80 and 160 °C for 6 h each. The resulting powders were added to a sucrose solution [13.5 g of sucrose, 108 g of H_2O, and 1.44 g of H_2SO_4 (98 wt %)] again for another impregnation cycle. After being treated again at 80 and 160 °C for 6 h as before, carbonization was carried out in a tube furnace at 900 °C for 2 h under nitrogen at a flow rate of 100 mL min^{-1}. Mesoporous silica hard template was then etched with 10 wt % HF aqueous solution. After being washed with ethanol and dried at 100 °C, 8.2 g of mesoporous carbon template (CMK-3) was collected.

2.3. Synthesis of SiC−C Nanocomposites. The synthetic procedure was carried out by an organic solvent evaporation impregnation method similar to that used in our previous report.[16] In this approach, 10.56 g of PCS was dissolved in 100 g of xylene to obtain a homogeneous solution. Then, 8.00 g of mesoporous carbon CMK-3 host was mixed well with the solution under stirring. When the xylene had nearly evaporated, the product was dried in an oven at 80 °C for 24 h. The film (about 0.5 mm in thickness in the vessel with a diameter of 45 mm) that formed on the surface was peeled off. Loose powders of PCS−carbon nanocomposites (17 g) were collected. Each alumina boat was loaded with 2.0 g of PCS−carbon nanocomposite. Heating was carried out in a tube furnace with a multistep temperature program in nitrogen flow: (1) heating from room temperature to 350 °C at a rate of 5 °C min^{-1}, (2) heating from 350 to 700 °C at a rate of 1 °C min^{-1} for cross-linkage and pyrolysis of PCS, (3) heating from 700 °C to the final pyrolysis temperature (900−1500 °C) at a rate of 2 °C min^{-1}, (4) maintenance of the terminal temperature for 30 min, and (5) cooling to room temperature. The mesostructured SiC−C products are denoted as SiC−C-*X*, in which *X* represents the final pyrolysis temperature. In all cases, about 1.72 g of SiC−C composite was obtained.

2.4. Air-Assisted in Situ Transformation from SiC−C to SiOC. To obtain SiOC, SiC−C-*X* samples were directly heated at 500 °C for 10 h under air atmosphere in a Muffle furnace. The mesoporous products are denoted as SiOC-*X*, where *X* indicates the final pyrolysis temperature of the corresponding SiC−C-*X* nanocomposites. In each in situ transformation experiment, the initial weight of mesostructured SiC−C nanocomposite was 0.150 g.

2.5. Ammonia-Assisted in Situ Transformation from SiC−C to SiCN. Ammonia gas-assisted synthesis was utilized to transform mesostructured SiC−C in situ into mesoporous SiCN ceramics. The first step of heating the SiC−C-*X* samples, to 1000 °C, was carried out in an alumina boat under a high-purity nitrogen flow (50 mL min^{-1}). Then, ammonia gas was fed at a flow rate of 250 mL min^{-1}. The temperature was maintained for 10 h. Finally, the flow was switched again to high-purity nitrogen for cooling to room temperature. The derived mesoporous products are denoted as SiCN-*X*, where *X* has the same value as in the parent mesostructured SiC−C-*X* material.

2.6. Characterization. Powder X-ray diffraction (XRD) patterns were recorded on a Bruker D4 X-ray diffractometer with Ni-filtered Cu Kα radiation (40 kV, 40 mA). Small-angle X-ray scattering (SAXS) measurements were obtained on a Nanostar U small-angle X-ray scattering system (Bruker) using Cu Kα radiation (40 kV, 35 mA). The *d* spacing values were calculated with the formula $d = 2\pi/q$, and the unit cell parameters were calculated with the formula $a = 2d_{100}/\sqrt{3}$. Nitrogen sorption isotherms were measured on a Micromeritics Tristars 3000 analyzer at −196 °C. Before the measurements, the samples were outgassed at 160 °C in a vacuum for 6 h. The Brunauer−Emmett−Teller (BET) method was utilized to calculate the specific surface areas. The pore size distributions were derived from the adsorption branches of the isotherms using the Barrett−Joyner−Halenda (BJH) method. The total pore volumes, V_p, were estimated from the amount adsorbed at a relative pressure of $P/P_0 = 0.98$. Transmission electron microscopy (TEM) measurements were conducted on a JEOL 2011 microscope operated at 200 kV. All samples were first dispersed in ethanol and then collected using carbon-film-covered copper grids for analysis. The oxygen and nitrogen contents of the products were determined using a TC600 Nitrogen/Oxygen Determinator (LECO). The contents of silicon and carbon were determined by chemical analysis. Thermogravimetric (TG) analyses were carried out on a Mettler Toledo TGA/SDTA851 apparatus under an air flow at a rate of 150 mL min^{-1}. ^{29}Si solid-state NMR experiments were performed on a Bruker DSX300 spectrometer (Rheinstetten, Germany) under the conditions of cross-polarization (CP) and magic-angle sample spinning (MAS). The spectra were collected at room temperature at a frequency of 59.6 MHz, a cycling delay of 900 s, a radiation frequency intensity of 62.5 kHz, and a reference sample of Q_8M_8 ($[(CH_3)_3SiO]_8Si_8O_{12}$).

3. Results

3.1. Hard Template: Mesoporous Silica and Mesoporous Carbon. The XRD pattern (Figure 1a) of mesoporous silica SBA-15 shows five resolved diffraction peaks, which can be indexed in turn to the 100, 110, 200, 210, and 220 reflections of *p6mm* symmetry. TEM images (not shown) also reveal a two-dimensional (2-D) hexagonal mesostructure with a high structural regularity in large domains.

Mesoporous silica SBA-15 was subsequently used as a hard template to replicate ordered mesoporous carbon CMK-3. This was the first nanocasting step. After the mesoporous silica hard template had been etched, three well-resolved diffraction peaks could be detected in the XRD pattern

(34) Zhao, D. Y.; Feng, J. L.; Huo, Q. S.; Melosh, N.; Fredrickson, G. H.; Chmelka, B. F.; Stucky, G. D. *Science* **1998**, *279*, 548.
(35) Ryoo, R.; Joo, S. H.; Jun, S. *J. Phys. Chem. B* **1999**, *103*, 7743.

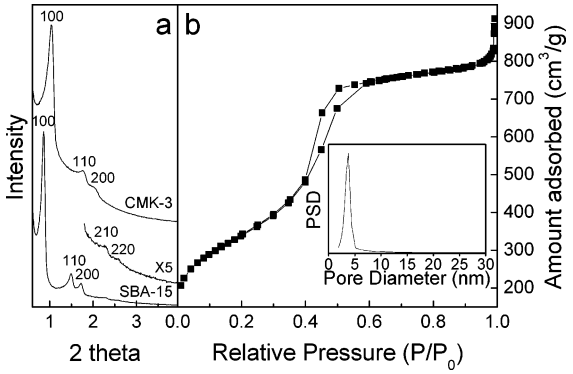

Figure 1. (a) Small-angle XRD patterns of mesoporous silica SBA-15 and carbon CMK-3 templates. (b) Nitrogen sorption isotherms of mesoporous carbon CMK-3 template. The inset in part b is the pore size distribution.

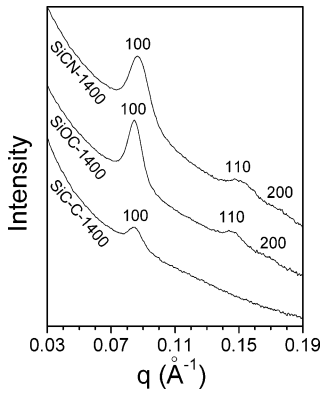

Figure 2. SAXS patterns for mesostructured SiC−C-1400 composite and mesoporous SiOC-1400 and SiCN-1400 ceramics that were transformed in situ from SiC−C-1400 by heating at 500 °C for 10 h in air and at 1000 °C for 10 h in ammonia atmosphere, respectively.

(Figure 1a). This indicates a highly ordered 2-D hexagonal mesostructure. TEM measurements also revealed that the mesoporous carbon had ordered hexagonally arranged nanorod arrays, as reported in the literature. Nitrogen sorption isotherms (Figure 1b) showed that the resulted mesoporous carbon had a total pore volume of 1.2 g cm^{-3}, a BET surface area of 1200 m^2 g^{-1}, and a pore diameter of 3.8 nm with a narrow distribution.

3.2. Mesostructured SiC−C Nanocomposites. A second nanocasting step was introduced to prepare SiC−C nanocomposites using mesoporous carbon as the hard template and PCS as the precursor. On the basis of the pore volume of mesoporous carbon and the density of PCS (1.1 g cm^{-3}), the experimental recipe of PCS can be ideally filled in the nanospace of mesoporous carbon template (1.32 g of PCS/1.0 g of carbon). The obtained PCS−C nanocomposite was in the form of a compact powder, implying that the precursor was mainly filled inside the mesopores of the carbon template.

Heating the dried PCS−C sample according to the described procedure gave rise to SiC−C nanocomposites because of the pyrolysis of the PCS. The SAXS pattern of the collected SiC−C nanocomposites after pyrolysis at 1400 °C is shown in Figure 2. Only one weak scattering peak can be detected, indexed to the 100 reflection of the hexagonal *p*6*mm* mesostructure. This is common for guest-filled mesoporous materials obtained by the nanocasting strategy and can be ascribed to the decrease of contrast in the mesostructure caused by the presence of SiC inside the nanospace of CMK-3.

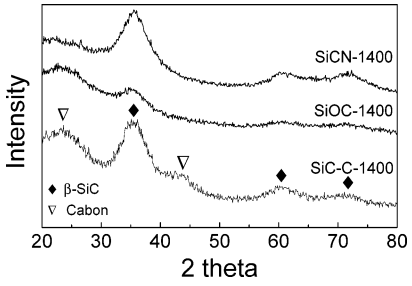

Figure 3. XRD patterns of mesostructured SiC−C-1400 composite and mesoporous SiOC-1400 and SiCN-1400 ceramics.

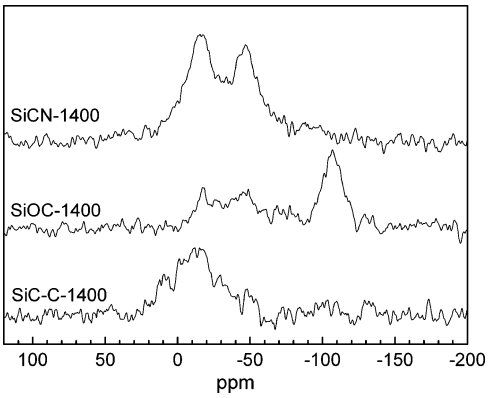

Figure 4. ^{29}Si NMR spectra of mesostructured SiC−C-1400 nanocomposite and mesoporous SiOC-1400 and SiCN-1400 ceramics.

The wide-angle XRD pattern (Figure 3) for SiC−C-1400 nanocomposite displays five diffraction peaks. Two broad peaks at 2θ values of 24 and 43° correspond to the 002 and 10 lattice planes of amorphous carbons, respectively. These arise from the carbon template and the pyrolysis byproducts of PCS. The other three broad diffraction peaks appear at 2θ values of 35.5, 60.1, and 71.1° and can be indexed as the 111, 200, and 311 reflections, respectively, of β-SiC crystallites. This suggests the low extent of crystallization of SiC and the coexistence of amorphous carbon in the nanocomposite.

The ^{29}Si NMR spectrum (Figure 4) of the SiC−C composites after pyrolysis at 1400 °C shows a broad signal in the range from −70 to 20 ppm, which is typical for SiC pyrolyzed by PCS precursor.[17,36] Two shoulder peaks are also observed at around 10 and −50 ppm, suggesting the formation of SiC_3O and SiC_2O_2, respectively.[17,36] These oxygen atoms might originate from a large amount of adsorbed water because of the large surface areas of these mesoporous materials and the residual oxygen in the carbon templates.

3.3. Mesoporous SiOC: Air-Assisted in Situ Transformation. The SiC−C-1400 nanocomposite was first heated at 500 °C for 10 h in air to transform it to SiOC and remove the carbon template. Elemental analysis showed that the product (SiOC-1400) was composed of 46.2 wt % Si, 46.3 wt % O, and 7.5 wt % C, giving the stoichiometric composition of $Si_1O_{1.75}C_{0.38}$. The wide-angle XRD pattern

(36) Williams, H. M.; Dawson, E. A.; Barnes, P. A.; Rand, B.; Brydson, R. M. D.; Brough, A. R. *J. Mater. Chem.* **2002**, *12*, 3754.

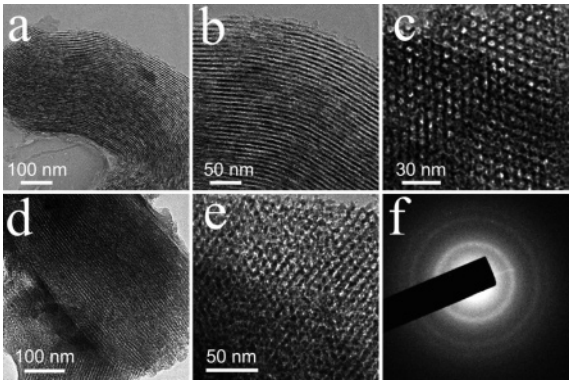

Figure 5. TEM images of mesoporous SiOC-1400 at (a) low magnification and (b, c) high magnification taken along the (b) [110] and (c) [100] directions. TEM images of mesoporous SiCN-1400 taken along the (d) [110] and (e) [100] directions. (f) Selected-area electron diffraction (SAED) pattern of mesoporous SiCN-1400.

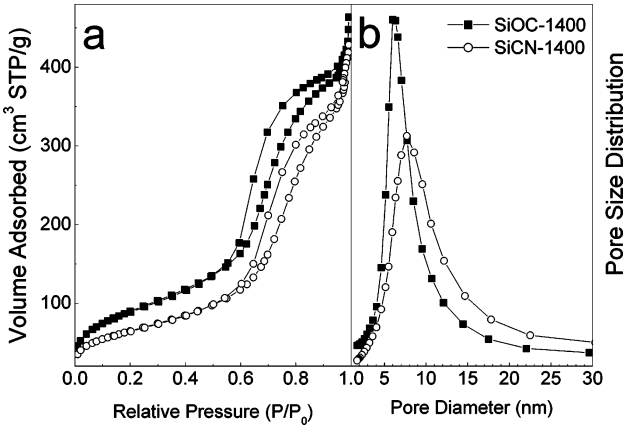

Figure 6. (a) Nitrogen sorption isotherms and (b) pore size distribution curves for mesoporous SiOC-1400 and SiCN-1400 ceramics after air- and ammonia-assisted in situ transformations of mesostructured SiC−C-1400 at 500 °C for 10 h and at 1000 °C for 10 h, respectively.

of SiOC-1400 (Figure 3) exhibited a large difference from that of its parent nanocomposite SiC−C-1400. The diffraction peaks corresponding to amorphous carbon disappeared, and those belonging to β-SiC were obviously weakened. A diffraction peak at a 2θ value of around 22° appeared that can be attributed to amorphous silica. Compared to SiC−C-1400, SiOC-1400 exhibits a strong signal at around −107 ppm and broad signals between −90 and 0 ppm in the ^{29}Si NMR spectrum (Figure 4). The former peak can be assigned to Q-type units (SiO_4-H_n). This indicates the formation of amorphous silica, in agreement with the XRD results. The latter broad signal suggests the maintenance of SiC_xO_y after the removal of the carbons.[21,22] These results suggest the complete oxidation of amorphous carbon and the reaction of partial SiC with air to form SiOC ceramics.

Compared to its parent SiC−C nanocomposite, the SiOC-1400 material displays a well-resolved SAXS pattern (Figure 2). Three resolved scattering peaks can be observed, indexed as the 100, 110, and 200 reflections of the 2-D hexagonal *p*6*mm* symmetry. The d_{100} value was calculated to be 7.46 nm. This suggests that these samples have ordered 2-D hexagonal mesostructure.

Ordered structural regularity was found in whole particles from the TEM images of SiOC-1400 (Figure 5). The typical stripelike and hexagonally arranged images, recorded at the [100] and [001] incidences, respectively, confirmed that SiOC-1400 exhibits an ordered 2-D hexagonal *p*6*mm* mesostructure. On the small scale, some stripes intermittent in pore walls can be found, indicating structure defects. The fringing spacing measured from Figure 5b is 7.3 nm, in good agreement with the value calculated from the SAXS pattern. This indicates that the mesoporous silica SBA-15 framework was transformed into a mesoporous SiOC framework via the combination of casting-by-casting process with mesoporous carbon as the intermediate and air-assisted in situ transformation.

Nitrogen sorption isotherms of SiOC-1400 ceramics (Figure 6) showed typical type-IV curves with a distinct capillary condense, indicative of uniform mesopores. It was found that the hysteresis loop was H_2-type, implying the presence of imperfect cylindrical channels. The BET surface area, pore size, and total pore volume were found to be 327 $m^2\ g^{-1}$, 6.2 nm, and 0.72 $cm^3\ g^{-1}$, respectively. The generation of the mesoporosity further suggests the removal of amorphous carbons that occupy the channels of the nanocomposite.

3.4. Mesoporous SiCN: Ammonia-Assisted in Situ Transformation. In addition to oxidative gases, reductive gases such as ammonia can also be employed in carbon template removal because they can reduce carbon to gaseous HCN and hydrogen.[24] The reaction rate is fairly high owing to the dissociation of ammonia into N and H radicals at a high temperature.

The second route to transform mesostructured SiC−C-1400 in situ was then carried out at 1000 °C for 10 h under ammonia gas. The product (SiCN-1400) was characterized by elemental analysis and wide-angle XRD. Elemental analysis showed that the product was composed of 54.5 wt % Si, 21.2 wt % C, 11.6 wt % N, and 12.6 wt % O, i.e., $Si_1C_{0.91}N_{0.42}O_{0.40}$. This demonstrates the incorporation of N into the SiC compound. Simultaneously, O was found to be included in the ceramics, although no oxygen was introduced to this system. This is similar to mesoporous BN[24] and SiCN,[20] which contain 21 and 9 wt % oxygen, respectively. The ^{29}Si NMR spectrum (Figure 4) of the obtained mesoporous SiCN-1400 shows two signals at −50 and −16 ppm that can be attributed to SiN_4 and SiC_4 units, respectively.[37,38] This result gives further evidence for the formation of carbonitrides (SiCN).

The diffraction peaks related to amorphous carbon disappeared in the wide-angle XRD pattern of SiCN-1400, indicating the complete removal of amorphous carbons. In contrast, the diffraction peaks corresponding to β-SiC remained almost unchanged after the reduction in ammonia gas (Figure 3), suggesting the low extent of crystallinity. The former phenomenon is analogous to that for SiOC-1400, but the latter is contrary to that of SiOC-1400, in which the patterns ascribed to β-SiC weakened after oxidation. This implies that reduction is more suitable than oxidation for stabilizing SiC-based ceramics.

(37) Schiavon, M. A.; Sorarù, G. D.; Yoshida, I. V. P. *J. Non-Cryst. Solids* **2002**, *304*, 76.
(38) Sung, I. K.; Christian, Mitchell, M.; Kim, D. P.; Kenis, P. J. A. *Adv. Funct. Mater.* **2005**, *15*, 1336.

As for mesoporous SiOC, the SAXS pattern of SiCN ceramics becomes more resolved after the ammonia treatment process and reveals a highly ordered *p*6*mm* mesostructure and a d_{100} value of 7.29 nm. However, the scattering peaks are somewhat broader than in the former, suggesting that the mesostructure ordering is slightly lower. Nitrogen sorption isotherms of the SiCN-1400 product are similar to those of SiOC-1400, indicating the generation of uniform mesopores and imperfect hexagonal channels. Mesoporous SiCN-1400 has a BET surface area of 231 $m^2\ g^{-1}$, a pore size of 7.6 nm, and a pore volume of 0.66 $cm^3\ g^{-1}$. By comparison, the pore size distribution of mesoporous SiCN-1400 is somewhat wider than that of SiOC-1400. TEM images of SiCN-1400 are similar to those of mesoporous silica SBA-15, revealing a 2-D hexagonal ordered mesostructure with open, continuous frameworks in large domains. The fringe spacing is 7.3 nm, in accordance with that estimated from the SAXS pattern. The intermittent stripe pattern can also be found in the wall of SiCN-1400, indicative of interwall connections. This phenomenon is more severe than that for mesoporous SiOC-1400, reflecting the slightly lower mesoscopic regularity of the former, in agreement with the results from the SAXS patterns and N_2 adsorption isotherms. This can be attributed to the higher carbon removal temperature and the lower ceramic yield for mesoporous SiCN-1400 than for SiOC-1400. The SAED pattern of SiCN-1400 (Figure 5f) displays three diffraction rings assigned to the 111, 220, and 311 planes of β-SiC. This is in agreement with the wide-angle XRD pattern and provides further evidence that the mesostructure is partially composed of β-SiC crystallites with random orientations.

3.5. Heating Procedure for the in Situ Transformation. The heating temperature and time are extremely important for the in situ transformation. For example, upon treatment of the obtained mesostructured SiC−C composite at 800 °C under air atmosphere, only mesoporous silica can be obtained through complete oxidation. During heating at 400 °C for 10 h, no mesoporosity can be achieved, because of insufficient carbon removal. Unfortunately, these parameters are neglected in most work. Here, we show a step-by-step choice. The elimination of amorphous carbon is a good evaluation for this step because it accompanies the transformation from mesostructured SiC−C to SiOC ceramics and generates mesoporosity.

To find appropriate conditions for the heat treatment, TG analysis of SiC−C-1400 was first carried out from 25 to 900 °C at a ramp of 5 °C min^{-1} under air flow. The TGA curve (Figure 7) shows four steps of weight change. The first minimum weight loss occurs below 270 °C, corresponding to the desorption and removal of water or other adsorbents. The second step is a weight increase of 2.5% ranging from 270 to 510 °C, owing to the oxidation of the SiC surface. The following large weight loss (46.6%) between 510 and 700 °C is attributed to the combustion of amorphous carbons, including the carbon template and the excess carbon from the pyrolysis byproducts of PCS. Finally, a fourth weight increase above 700 °C is related to the further oxidation of the SiC frameworks. The residue weight is about 52.5%.

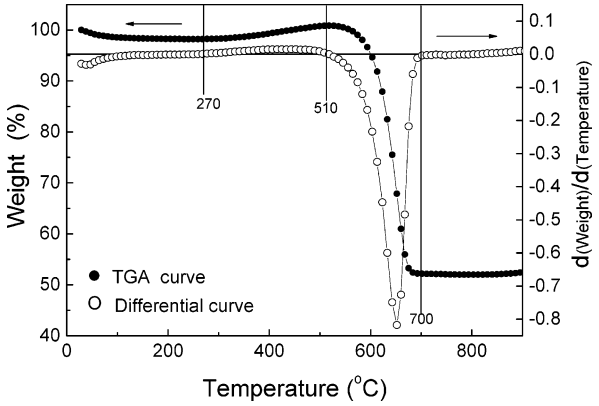

Figure 7. TGA curve of SiC−C-1400 nanocomposite under air flow and the corresponding differential curve.

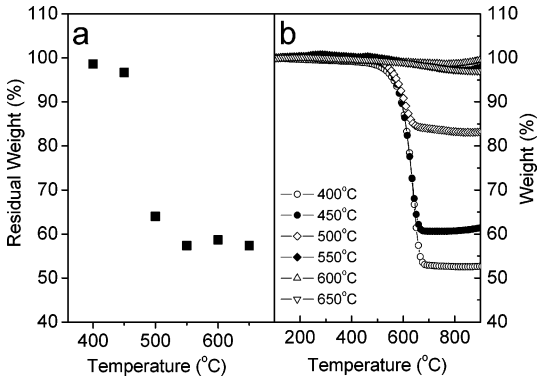

Figure 8. (a) Residual weight ratios of the samples derived from treating SiC−C-1400 nanocomposite at temperatures between 400 and 650 °C for 5 h in air compared to the initial SiC−C-1400 nanocomposite and (b) their corresponding TGA curves.

According to the TGA results, mesostructured SiC−C-1400 was heated at temperatures between 400 and 650 °C in intervals of 50 °C. The heating time was 5 h in each experiment. Figure 8a shows a plot of the residual weight ratios of the resulting samples. No obvious weight loss can be detected for the samples heated below 450 °C. Further increasing the temperature to 500 °C leads to a dramatic consumption, suggesting a notable improvement in the gasification of carbon. However, the residual weight is higher than that from the TGA analysis, and the color of the product is still black, indicating the incomplete elimination of amorphous carbon. As the heating temperature is increased to 550 °C or above, the residual weights are maintained at about 58%, and the color of the products changes to khaki. These phenomena demonstrate the complete removal of amorphous carbon and the formation of SiC-based ceramics.

TGA curves (Figure 8b) of these resultant SiC-based ceramics were collected to further evaluate the elimination of amorphous carbon. The materials produced below 500 °C exhibit a large weight loss between 510 and 700 °C. For example, a weight loss of about 47% was detected in the TGA test of the sample heated at 400 °C, the same as that for mesostructured SiC−C-1400. This behavior reveals the presence of a large amount of amorphous carbon in these samples. The proportion of amorphous carbon in the sample heated at 500 °C significantly decreases, as evidenced by the comparatively small weight loss in the TGA curve. In

the cases of the samples calcinated at 550 °C or above, no sharp weight loss can be detected, confirming the complete oxidation of amorphous carbon and template removal.

On the considerations of carbon elimination and moderate process conditions, the temperature of 500 °C was chosen for the air-assisted transformation. The next step was to investigate the effect of calcination time. The air-assisted transformation experiments for SiC−C-1400 were carried out at 500 °C for 2−12 h. The colors of the samples were black, black, jet black, gray, French gray, and khaki, corresponding to heating time of 1, 2.5, 6, 7.5, 9, and 12 h, respectively (Supporting Information Figure S1). The residual weight distinctly decreased with increasing time and tended to a constant for a heating time of 10 h (Figure S2). TGA tests (Figure S3) were then performed on these products under air. The sample heated for 1 h displayed a sharp weight loss in the temperature range of 510−700 °C corresponding to the removal of amorphous carbon with a residue of 53.5%, as for mesostructured SiC−C-1400. When the heating time was increased to 2.5, 6, and 7.5 h, the weight losses were 42%, 17%, and 9%, respectively. TGA curves showed undetectable weight loss for samples heated for more than 9 h. These results indicate the inefficiency for removing amorphous carbon in mesostructured SiC−C at 500 °C within an insufficient time. Calcination at 500 °C for 10 h under air can deplete amorphous carbon and give rise to template-free mesoporous SiOC materials. It is interesting that the residue weight after the air-assisted transformation at 500 °C for 10 h was about 55%, lower than those prepared at 550 and 600 °C for 5 h. This phenomenon might be related to a more moderate oxidation and a lower yield of silica at lower temperatures. Therefore, the temperature of 500 °C and the time of 10 h were adopted in the air-assisted in situ transformation experiments from the SiC−C composites to mesoporous SiOC ceramics.

As for the SiOC materials, a series of SiCN samples were collected by directly heating SiC−C-1400 at temperatures ranging from 800 to 1200 °C for 10 h under ammonia. The weight change was minor for the samples treated at temperatures lower than 1000 °C (Figure S4). When the heating temperature reached at 1000 °C, the residue weight declined to about 50%. This phenomenon, together with the color change from black to French gray (Figure S5), is evidence for the complete reduction of amorphous carbon. A fluctuation instead of a continuous decrease occurs at higher reduction temperatures, confirming the depletion of amorphous carbon.

When the reduction temperature in the ammonia treating process for mesostructured SiC−C was lower than 1000 °C, the TGA curves (Figure S6) of the collected products exhibited a steep step in the temperature range of 510−700 °C, indicating a great deal of amorphous carbon. This implies that temperatures below 1000 °C play a minor role in the reductive reaction. The large weight loss in the TGA curves disappeared for the samples heated at 1000 °C or above, suggesting the complete removal of the carbon templates. This further reveals that the heating temperature dramatically influence the final products. The temperature of 1000 °C and the time of 10 h under the present ammonia-assisted conditions were sufficient to fully reduce and remove the amorphous carbon.

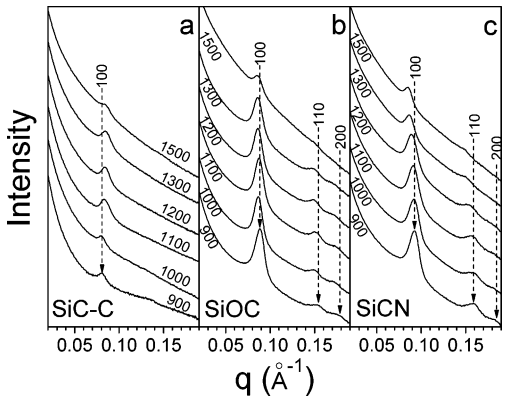

Figure 9. SAXS patterns of (a) mesostructured SiC−C nanocomposites heated at different temperatures and the corresponding derivations of (b) mesoporous SiOC via air-assisted in situ transformation at 500 °C for 10 h and (c) mesoporous SiCN via ammonia-assisted in situ transformation at 1000 °C for 10 h.

Table 1. Textural Properties of Mesoporous Silica and Carbon Template, SiC−C Nanocomposites, and Mesoporous SiOC and SiCN Products Prepared under Different Conditions

sample	d_{100} spacing (nm)	cell parameter a (nm)	BET surface area ($m^2\ g^{-1}$)	pore diameter (nm)	pore volume ($cm^3\ g^{-1}$)
SBA-15	10.27	11.86	742	7.3	0.93
CMK-3	8.58	9.91	1200	3.8	1.20
SiC−C-900	7.85	9.07	–	–	–
SiC−C-1000	7.82	9.03	–	–	–
SiC−C-1100	7.55	8.72	–	–	–
SiC−C-1200	7.49	8.64	–	–	–
SiC−C-1300	7.46	8.61	–	–	–
SiC−C-1400	7.52	8.68	–	–	–
SiC−C-1500	7.52	8.68	–	–	–
SiOC-900	7.10	8.19	386	4.9	0.44
SiOC-1000	7.27	8.40	391	5.4	0.52
SiOC-1100	7.18	8.29	347	5.2	0.61
SiOC-1200	7.30	8.43	422	5.6	0.74
SiOC-1300	7.33	8.46	410	5.6	0.76
SiOC-1400	7.46	8.61	327	6.2	0.72
SiOC-1500	7.39	8.54	251	8.4	0.73
SiCN-900	6.82	7.87	274	5.2	0.43
SiCN-1000	6.85	7.91	299	5.0	0.46
SiCN-1100	6.93	8.00	255	5.6	0.45
SiCN-1200	7.10	8.19	272	5.8	0.59
SiCN-1300	7.24	8.36	234	6.0	0.54
SiCN-1400	7.29	8.42	233	7.6	0.66
SiCN-1500	7.39	8.54	205	10.3	0.81

3.6. Effect of Pyrolysis Temperature on SiC-Based Ceramics. The SAXS patterns for SiC−C nanocomposites after pyrolysis at different temperatures ranging from 900 to 1500 °C are shown in Figure 9a. The corresponding d_{100} spacings and cell parameters are listed in Table 1. One can observe only one weak peak in each SAXS pattern, related to the 100 reflection of the 2-D hexagonal mesostructure. As mentioned above, this phenomenon can be assigned to the low contrast of the mesostructure owing to the occupation of the nanospace by different solids. Simultaneously, the q value of the nanocomposite shifted to a higher value, and the cell parameter decreased from 9.07 to 8.68 nm as the pyrolysis temperature increased. This phenomenon suggests that the periodic scale of the mesostructure shrank after the high-temperature treatment.

The wide-angle XRD patterns (Figure 10) of SiC−C nanocomposites after pyrolysis below 1200 °C showed only

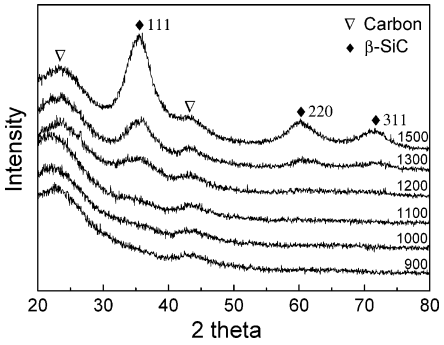

Figure 10. Powder XRD patterns of mesostructured SiC−C nanocomposites synthesized at temperatures ranging from 900 to 1500 °C.

two broad diffraction peaks at 2θ values of 24 and 43°, which can be attributed to the 002 and 10 planes, respectively, of amorphous carbons. No obvious diffraction peaks from SiC crystals could be observed. The emergence of a diffraction peak at a 2θ value of 35.5°, together with two other peaks at 2θ values of 60.1° and 71.7° in SiC−C-1300, confirms the formation of SiC. In contrast, the Bragg diffractions of amorphous carbons remained almost constant, suggesting the stability of amorphous carbons in the experimental temperature range.

After the air- and ammonia-atmosphere in situ transformation, the products (SiOC and SiCN materials) exhibited more resolved SAXS patterns (Figure 9b and c), which can be ascribed to the increase in contrast after the carbon template was removed from the nanocomposite. The SAXS patterns exhibit 2-D hexagonal scattering peaks, suggesting an ordered mesostructure with *p*6*mm* symmetry. Increasing the pyrolysis temperature of the parent mesostructured SiC−C nanocomposites from 900 to 1400 °C did not obviously influence the structural regularity of the SiOC and SiCN products prepared by the atmosphere-assisted transformation. However, the cell parameters ranged from 8.19 to 8.61 nm for mesoporous SiOC ceramics and from 7.87 to 8.42 nm for mesoporous SiCN ceramics, depending on the pyrolysis temperatures of their parent nanocomposites. The SAXS patterns of SiOC-1500 and SiCN-1500 were extremely weak.

Nitrogen sorption isotherms of the resulting SiOC and SiCN ceramics (Figure 11a and c) exhibit typical type-IV curves with a distinct capillary condense, which indicates uniform mesopores. The central position of this step shifts from about 0.5 to 0.9 for SiC-based ceramic products with an increase in the pyrolysis temperature of their parent mesostructured SiC−C nanocomposites from 900 to 1400 °C. This exhibits an ascending order for the pore sizes of mesoporous SiOC and SiCN ceramics. The pore size distributions curves (Figure 11b and d) confirm these results. The mean pore diameter is enlarged from 4.9 to 6.2 nm for mesoporous SiOC and from 5.2 to 7.6 nm for mesoporous SiCN as a function of the initial pyrolysis temperature of the parent nanocomposites. It was found that the hysteresis loops are H_2-type, implying imperfect cylindrical channels. The BET surface areas and the total pore volumes of mesoporous SiOC ceramics were about 320−420 $m^2\ g^{-1}$ and about 0.4−0.8 $cm^3\ g^{-1}$ (Table 1), respectively, except for SiOC-1500. The latter had a low BET surface area of 250 $m^2\ g^{-1}$. Mesoporous SiCN ceramics had BET surface areas

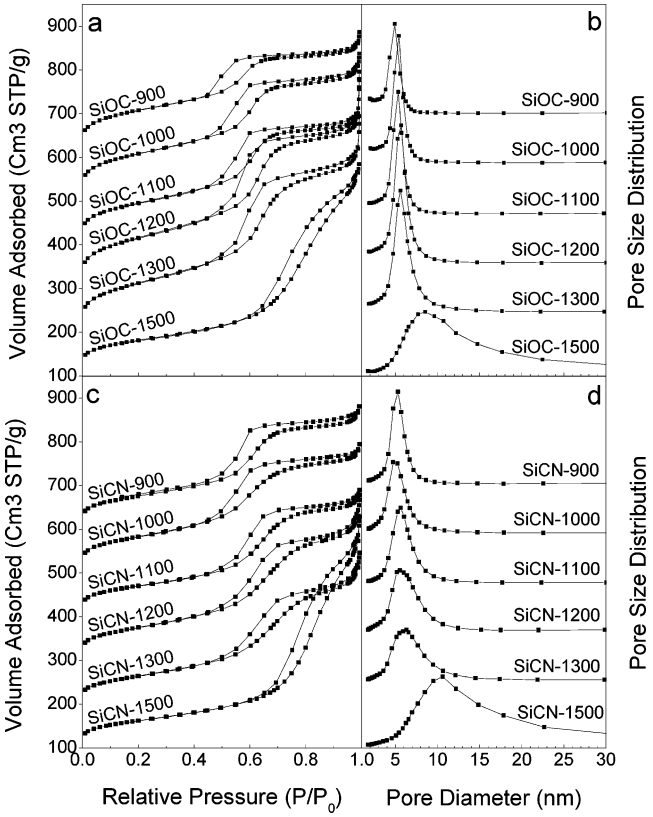

Figure 11. (a,c) Nitrogen sorption isotherms and (b,d) pore-diameter distribution curves of (a,b) mesoporous SiOC and (c,d) SiCN ceramics derived from different SiC−C nanocomposites. Each isothermal curves is offset along the *y* axis by 100 $cm^3\ g^{-1}$ relative to the previous curve.

of about 230−300 $m^2\ g^{-1}$ and pore volumes of about 0.4−0.7 $cm^3\ g^{-1}$. The BET surface area of the SiCN-1500 sample was only 205 $m^2\ g^{-1}$.

Mesoporous SiOC-1500 and SiCN-1500 showed weak X-ray diffractions and low BET surface areas, which might be related to poor mesoscopic regularity and too many voids inside the pore walls. The collapse of the mesostructure might be inherited from the parent SiC−C nanocomposite. Although carbon is stable at 1500 °C, mesoporous carbon CMK-3 is not a continuous framework and is constructed of a nanorod array. Some random small pillars connect the carbon nanorods to form the ordered arrangement. The growth of the β-SiC crystallite and the squeezing of carbon nanorods around the crystallites are aggravated with increasing temperature, which might somewhat destroy the mesostructure. As a result, a large amount of interconnections between cylinder pores are generated. It was noticed that the pore sizes of mesoporous SiOC-1500 and SiCN-1500 ceramics were almost the same as or larger than their cell parameters. Similar phenomena have been observed in mesotunneled 3D-SBA-15 and mesoporous silica from mesoporous silica−carbon nanocomposites.[29,39] The large mesopore tunnels (>4 nm) on pore walls can contribute space for nitrogen condensation in the isotherms, reflecting a large calculated pore size and a wide pore size distribution. Therefore, mesostructured SiC−C with an initial pyrolysis temperature of 1400 °C is a suitable parent nanocomposite

(39) Fan, J.; Yu, C. Z.; Wang, L. M.; Tu, B.; Zhao, D. Y.; Sakamoto, Y.; Terasaki, O. *J. Am. Chem. Soc.* **2001**, *123*, 12113.

for the derivation of ordered mesoporous SiOC and SiCN ceramics with good crystallinity by the present atmosphere-assisted in situ transformation.

4. Discussion

Highly ordered mesoporous silica SBA-15 synthesized using P123 as a structure-directing agent (SDA) has an open, continuous framework. It can be used as a hard template for the fabrication of highly ordered mesoporous carbon with a reversed structure. The second nanocasting step is accomplished by using mesoporous carbon as a hard template and commercially available PCS as a precursor to obtain PCS−C nanocomposites.

The loading amount of the PCS precursor is very important in the nanocasting process: Insufficient infiltration would cause poor structure ordering, whereas an excess would result in serious agglomeration. The optimal ratio in our experiments was found to be 1.32 g of PCS/1.0 g of carbon. This happens to represent 100% filling of PCS molecules inside the pore voids of the carbon templates calculated from the nitrogen sorption data. However, we believe that not all PCS molecules can infiltrate into the nanospace in this case. The ideal volume is larger than the space that PCS molecules can reach. This is due to the facts that nitrogen is smaller than PCS and some micropores can be filled by nitrogen but cannot be occupied by PCS molecules. In our experiments, PCS molecules outside the mesochannels were indeed observed. They appeared as a thin film that covered the surface of the loose powders. Although the formation of this thin film is apparently related to use of excess precursor to some extent, it cannot be limited to this reason. Such a film could be found on the surface of the infiltrated powders after drying even when the amount of PCS was reduced by 50%, namely, to 0.66 g of PCS/1.0 g of carbon. Below this is the loose PCS−C composite powders. A similar phenomenon was found when the infiltration amount of PCS did not exceed 1.32 g of PCS/1.0 g of carbon. The thickness of the film remained at about 0.5 mm. Further applying a 10% higher dose of PCS did not make the film thicker, but led to a serious agglomeration of the overall powder samples after drying, suggesting that excess PCS remained at the outer surface of the mesoporous carbons. These results imply that the formation of the film on the surface is not related to the presence of excess precursor. In addition, the infiltrated product was dried in an oven at 80 °C for 24 h when xylene was nearly evaporated. The direct contact of the surface of the sample with hot air might result in the extreme evaporation of xylene. Therefore, the surface of the sample was quickly solidified, leading to the formation of a thin film. In this film, some PCS indeed located outside the mesochannels and connected the particles together. The film could thus seal up the main powder body below it. The release of xylene would then become slower. On the other hand, the solubility of PCS in xylene is improved at 80 °C. Therefore, more PCS molecules would have enough time to diffuse into the mesochannels of carbon under the protection of this cover film.

The almost complete occupation of the nanospace of carbon by PCS also relies on the promoting interaction between the guest and the hard template. PCS molecules (SiR_2CH_2), with a silicon-altering carbon fundamental chain structure, contain a great number of C−H groups. Mesoporous carbon CMK-3 is a product from the nanocasting procedure using sucrose as the precursor. The C−H bonds can residue on the surface after carbonization. The molecular recognition or van der Waals interaction between the guest and the hard template would improve the filling amount to reach a maximum, fully occupying the nanospace inside the mesoporous carbon. By comparison, the optimal ratio is about 0.88 g of PCS per cm^3 of pore volume of silica if mesoporous silica is used as a hard template.[16] This difference can be attributed to the better wetting between PCS and the hydrophobic carbon surface than between PCS and the hydrophilic silica surface.

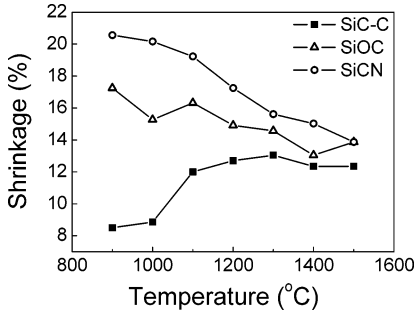

Figure 12. Relationship of mesostructure shrinkage of SiC−C, SiOC, and SiCN ceramics in cell parameters to the pyrolysis temperature of SiC−C nanocomposites.

Ordered mesostructured SiC−C composites were obtained by the pyrolysis of PCS and further crystallization. During this step, the heating temperature affected the crystallinity and mesostructure. With the elevation of temperature, the crystallinity of β-SiC increased. At the same time, the mesostructure shrank. On the basis of the d_{100} spacing, the shrinkage of the mesostructured SiC−C nanocomposites was calculated with the following formula

$$\text{shrinkage (\%)} = \frac{[d_{100}(\text{CMK-3}) - d_{100}(\text{SiC−C})]}{d_{100}(\text{CMK-3})} \times 100$$

which is plotted in Figure 12 as a function of temperature. A steadily shrinking domain size in SiC−C can be seen as the pyrolysis temperature increases. The structural shrinkage can be explained by the removal of free volume, in both the carbon template and the ceramic. Compared to that of mesostructured SiC−SiO_2 nanocomposites casted from mesoporous silica SBA-15,[16] the shrinkage of mesostructured SiC−C composites is relatively smaller. In the former case, the shrinkage is as large as 22% at 1400 °C,[16] almost 1.8 times that of SiC−C-1400. This difference can be attributed to the flexibility of silica and the rigidity of carbon.

Highly crystallized SiC materials are generally thermally stable (>800 °C) under air atmosphere and stable even at higher temperatures under ammonia atmosphere. A compact silica layer formed in the early stage of oxidation can inhibit the penetration of oxygen atoms and, hence, protect the materials from aggravating oxidation.[40] However, in the

(40) Filipuzzi, L.; Camus, G.; Naslain, R.; Thebault, J. *J. Am. Ceram. Soc.* **1994**, *77*, 459.

Scheme 1. Synthetic Approach for Mesoporous SiC-Based Ceramics by Atmosphere-Assisted in Situ Transformation

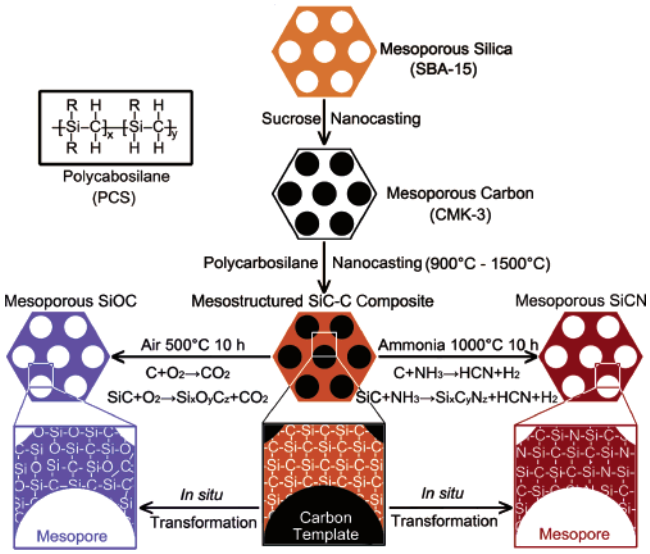

present case, mesostructured SiC preducts prepared by the casting-by-casting method exhibit poor oxidation and reduction resistance. This might be related to the ultrahigh surface areas of the mesoporous SiC frameworks. The low crystallinity might also be responsible for the poor oxidation resistance. Except for the diffraction from carbon templates, only three broad diffractions can be observed in the wide-angle XRD pattern of SiC−C-1500 with the highest crystallinity among the studied samples. Last, but not least, is the ultrathin pore walls. The thickness is lower than 4 nm. It is the reactive SiC framework that makes it possible to modulate the composition by treating mesostructured SiC−C under air and ammonia atmospheres. Amorphous SiOC and SiC in the SiC−C nanocomposites can react with oxygen or ammonia at high temperatures. Second, carbon templates contain about 7 wt % oxygen, which can be released during the carbon removal. This, together with the water impurity in ammonia, can oxidize SiC to form SiC_xO_y species. The Si−O bonds can then be substituted for Si−N bond by reacting with ammonia.[32] In addition, the bonding energies for Si−C, Si−N, and Si−O are 318, 355, and 452 kJ mol^{-1}, respectively.[41] Therefore, both oxygen and nitrogen can be incorporated into the covalent Si−C networks and substitute the carbon atoms.

A step-by-step choice shows that air-assisted oxidation at 500 °C for 10 h or ammonia-assisted reduction at 1000 °C for 10 h can transform mesostructured SiC−C to mesoporous SiOC or SiCN ceramics as a result of a gas−solid reaction, accompanied by the removal of amorphous carbons including the mesoporous carbon templates and the pyrolysis byproducts of PCS. The products have open, continuous frameworks. As shown in Scheme 1, the mesoporous silica SBA-15 framework is transformed into a mesoporous SiOC or SiCN framework with mesoporous carbon as the intermediate by the combination of the casting-by-casting procedure with the reactive atmosphere-assisted in situ transformation. An ordered mesostructure can be maintained to some degree, especially when the initial pyrolysis temperature for the SiC−C nanocomposites ranges from 900 to 1400 °C.

Compared to mesostructured SiC−C nanocomposites, the derived mesoporous SiOC and SiCN ceramics exhibit smaller cell parameters, indicative of a further structural shrinkage during the air or ammonia treament process (Figure 9). In contrast to the decreasing cell parameters of the composites, the cell parameters of the mesoporous SiOC and SiCN ceramics increase with a slight fluctuation as the pyrolysis temperature for the SiC−C nanocomposites rises. This implies that the shrinkage of the mesostructures from the atmosphere-assisted in situ transformation decreases. For example, the additional shrinkage of mesoporous SiCN-1400 is as small as 2.6%, almost 5 times less than that of SiCN-900 (12%). The increasing domain size in SiCN and in SiOC can be explained by the rigidity of the ceramic phase, again because of the difference in the free volume contents of samples pyrolyzed at different temperatures. During the ammonia (or air) treatment, the ceramic network can undergo viscous creep, under the driving force provided by surface tension. The higher the pyrolysis temperature of the SiC−C material, the lower the free volume content in the ceramic, the lower the amount of creep, and therefore the larger the domain size. Therefore, the resistance to structural shrinkage is improved during the subsequent air or NH_3 treatment process. At the same time, the pore sizes of mesoporous SiOC and SiCN materials exhibit the same increasing trend as the cell parameters, which might also be caused by the change in the rigidity of the ceramic phase. However, the rate of enlargement for the pore sizes is much faster than the latter. This can be attributed to the large amount of interconnections between the cylinder pores. Under the restriction that the impregnation amounts are the same for all samples, the enlargement of cell parameters thins the pore walls and expands the voids in the frameworks.

The resultant products of mesoporous SiOC and SiCN ceramics from the same SiC−C nanocomposites are much different in both composition and mesostructure because of the dissimilar treatment processes. After the gas−solid reaction, the wide-angle XRD patterns showed a significant difference between SiOC-1400 and SiCN-1400, suggesting that the Si−C bond network is more stable in ammonia than in air. In the former case, excess oxidation occurs, and a large amount of amorphous silica is formed during the air-assisted oxidation, as shown by XRD and ^{29}Si NMR results. In addition, the amount of nitrogen incorporated (11.6 wt %) in mesoporous SiCN is much less than the amount of oxygen incorporated in mesoporous SiOC (46.3 wt %) from the same SiC−C-1400 nanocomposite, even though the ammonia-assisted in situ transformation temperature (1000 °C) is much higher than the temperature of the air-assisted process (500 °C). These behaviors can be attributed to the dissimilarity in the bond energies. Owing to the large difference in treatment temperature, the cell parameters of mesoporous SiOC ceramics are systemically larger than those of SiCN materials originating from the same mesostructured SiC−C material. This implies less structural shrinkage for the former.

(41) Cottrell, T. L. *The Strengths of Chemical Bonds*, 2nd ed.; Butterworths: London, 1958.

5. Conclusions

Ordered mesoporous SiOC and SiCN ceramics with open and continuous frameworks have been fabricated by the combination of the casting-by-casting method with an atmosphere-assisted in situ transformation process. Mesostructured PCS−C nanocomposites were first casted from mesoporous carbon that was replicated from mesoporous silica. The pyrolysis of PCS and crystallization gave mesostructured SiC−C nanocomposites. The subsequent transformation involves the reaction of air and ammonia with SiC−C nanocomposites to form mesoporous SiOC and SiCN ceramics and the oxidation or reduction of carbons including the carbon templates and the pyrolysis byproducts of PCS. Our results show that the heating temperature and time of the atmosphere-assisted in situ transformation are crucial for the formation of ordered mesoporous SiOC and SiCN ceramics. A step-by-step choice reveals that the optimal temperature and time are 500 °C and 10 h and 1000 °C and 10 h, respectively, for air- and ammonia-assisted in situ transformations. The increase of the pyrolysis temperature from 900 to 1400 °C for SiC−C nanocomposites enhances the structural rigidity through the removal of free volume in both the carbon template and the ceramic and, therefore, reduces the structural shrinkage of the mesoporous SiOC and SiCN ceramics. The domain sizes of the SiOC and SiCN ceramics increase with increasing initial pyrolysis temperature. The SAXS, TEM, and N_2 sorption results show that mesoporous SiOC and SiCN frameworks have ordered 2-D hexagonal structures, high surface areas (200−400 $m^2\ g^{-1}$), large pore volumes (0.4−0.8 $cm^3\ g^{-1}$), and narrow pore size distributions (4.9−10.3 nm). Considering the reactive properties of active gases, such as hydrogen, sulfur, and chloride, the products from this general atmosphere-assisted in situ transformation process can therefore be extended to other mesoporous SiC-based ceramics by feeding these reactive gases into the system.

Acknowledgment. This work was supported by NSF of China (20421303, 20373013, 20407014, and 20521140450), State Key Basic Research Program of PRC (2006CB202502 and 2006CB0N0302), Shanghai Science & Technology Committee (03QF14037, 04JC14087, 05DZ22313, 055207078 and 06DJ14006), Shanghai Nanotech Promotion Center (0652nm024), Shanghai Leading Academic Discipline Project (T0402), Shanghai HuaYi Chemical Group, and Unilever Research Institute of China. Y.W. thanks China Post-Doc Scientific Fund.

Supporting Information Available: Photos, residual weight ratio data, and corresponding TGA curves of the samples derived from SiC−C-1400 by treating in air or ammonia under different treatment conditions. This material is available free of charge via the Internet at http://pubs.acs.org.

CM070283V